HAL
open science

Interrogating the ccm-3 Gene Network

Benjamin Lant, Swati Pal, Eric Michael Chapman, Bin Yu, Daniel Witvliet, Soo Choi, Lisa Zhao, Corinne Albigès-Rizo, Eva Faurobert, W. Brent Derry

To cite this version:

Benjamin Lant, Swati Pal, Eric Michael Chapman, Bin Yu, Daniel Witvliet, et al.. Interrogating the ccm-3 Gene Network. Cell Reports, 2018, 24 (11), pp.2857-2868.e4. 10.1016/j.celrep.2018.08.039 . hal-02335481

HAL Id: hal-02335481

https://hal.science/hal-02335481v1

Submitted on 28 Oct 2019

HAL is a multi-disciplinary open access archive for the deposit and dissemination of scientific research documents, whether they are published or not. The documents may come from teaching and research institutions in France or abroad, or from public or private research centers.

L'archive ouverte pluridisciplinaire **HAL**, est destinée au dépôt et à la diffusion de documents scientifiques de niveau recherche, publiés ou non, émanant des établissements d'enseignement et de recherche français ou étrangers, des laboratoires publics ou privés.

Distributed under a Creative Commons Attribution 4.0 International License

Article

Cell Reports

Interrogating the *ccm-3* Gene Network

Graphical Abstract

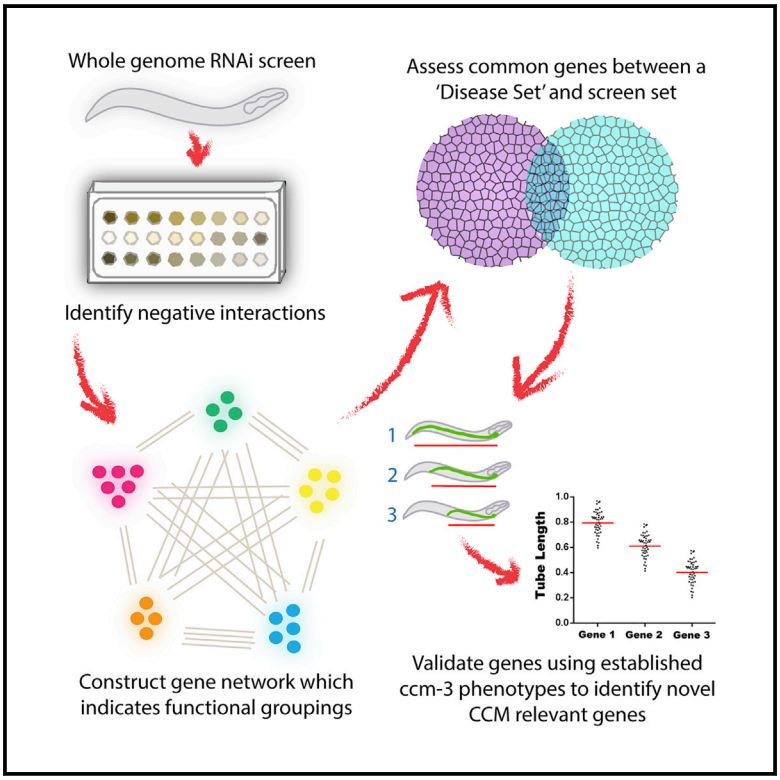

Highlights

- Over 500 cerebral cavernous malformation (CCM) modifier genes discovered in *C. elegans*
- Bioinformatics methods predict 29 conserved genes in core CCM-3/CCM3 network
- Many genes exhibit *ccm-3* phenotypes, including *mop-25.2*
- Loss of m*op-25.2* homolog MO25 causes stress fiber formation in endothelial cells

Authors

Benjamin Lant, Swati Pal, Eric Michael Chapman, ..., Corinne Albiges-Rizo, Eva Faurobert, W. Brent Derry

Correspondence

brent.derry@sickkids.ca

In Brief

Lant et al. use *C. elegans* genetics to better understand the human disease cerebral cavernous malformation (CCM). Through a whole-genome screen, and bioinformatics, they uncover a set of conserved genes that exhibit *ccm-3* phenotypes. These targets may be able to inform therapeutic studies.

Lant et al., 2018, Cell Reports *24*, 2857–2868
September 11, 2018 © 2018 Hospital for Sick Children.
https://doi.org/10.1016/j.celrep.2018.08.039

CellPress

Cell Reports
Article

OPEN ACCESS
CellPress

Interrogating the *ccm-3* Gene Network

Benjamin Lant,[1] Swati Pal,[1] Eric Michael Chapman,[1,2] Bin Yu,[1] Daniel Witvliet,[2,3] Soo Choi,[1,5] Lisa Zhao,[2] Corinne Albiges-Rizo,[4] Eva Faurobert,[4] and W. Brent Derry[1,2,6,*]
[1]Developmental and Stem Cell Biology Program, The Hospital for Sick Children, Peter Gilgan Centre for Research and Learning, 686 Bay Street, Toronto, ON M5G 0A4, Canada
[2]Department of Molecular Genetics, University of Toronto, 1 King's College Circle, Toronto, ON M5S 1A8, Canada
[3]Lunenfeld-Tanenbaum Research Institute at Mount Sinai Hospital, 600 University Avenue, Toronto, ON M5G 1X5, Canada
[4]Institute for Advanced Biosciences, CNRS UMR 5309, INSERM U1209, University Grenoble Alpes, Allée des Alpes, 38700 La Tronche, France
[5]Present address: Seoul National University, College of Medicine, 1 Gwanak-ro, Gwanak-gu, Seoul, South Korea
[6]Lead Contact
*Correspondence: brent.derry@sickkids.ca
https://doi.org/10.1016/j.celrep.2018.08.039

SUMMARY

Cerebral cavernous malformations (CCMs) are neurovascular lesions caused by mutations in one of three genes (*CCM1–3*). Loss of *CCM3* causes the poorest prognosis, and little is known about how it regulates vascular integrity. The *C. elegans ccm-3* gene regulates the development of biological tubes that resemble mammalian vasculature, and in a genome-wide reverse genetic screen, we identified more than 500 possible CCM-3 pathway genes. With a phenolog-like approach, we generated a human CCM signaling network and identified 29 genes in common, of which 14 are required for excretory canal extension and membrane integrity, similar to *ccm-3*. Notably, depletion of the MO25 ortholog *mop-25.2* causes severe defects in tube integrity by preventing CCM-3 localization to apical membranes. Furthermore, loss of *MO25* phenocopies *CCM3* ablation by causing stress fiber formation in endothelial cells. This work deepens our understanding of how *CCM3* regulates vascular integrity and may help identify therapeutic targets for treating *CCM3* patients.

INTRODUCTION

The nematode worm *Caenorhabditis elegans* contains several biological tubes, including multicellular tubes such as the intestine and germline as well as the unicellular excretory canals. Defects in the development or maintenance of these organs are often lethal to the organism or compromise its fitness. We recently developed *C. elegans* models of the neurovascular disease cerebral cavernous malformation (CCM) and discovered key roles for the worm *CCM3* gene, *ccm-3*, in promoting the extension and maintenance of excretory canals (Lant et al., 2015) and germline development (Pal et al., 2017). The function of CCM-3 is dependent on its protein binding partners within the striatin interacting phosphatase and kinase (STRIPAK) complex, and loss of *ccm-3* or STRIPAK genes causes defects in endocytic recycling and cytoskeletal organization (Lant et al., 2015; Pal et al., 2017). However, we lack a comprehensive understanding of how CCM-3/STRIPAK regulates these biological processes. Because of its genetic tractability and conservation of core CCM genes we took advantage of *C. elegans* to interrogate the CCM gene network.

CCM affects ~1 in 250 individuals and is caused by weak junctions in blood capillaries, which can leak blood into the brain parenchyma. This causes symptoms that range from mild headaches and seizures to hemorrhagic stroke, and it is not possible to predict when a lesion will bleed. The only treatment presently available for these patients is surgical resection, which can have devastating effects depending on lesion location. CCM can arise sporadically or, in approximately 40% of cases, by inheritance of mutations in one of the three CCM genes (*CCM1*/*KRIT1*, *CCM2*/*OSM*, and *CCM3*/*PDCD10*) (Fischer et al., 2013). These genes encode three distinct scaffold proteins that form a hetero-trimeric complex, in which loss of any one can cause activation of the small GTPase RhoA and stimulation of Rho kinase (ROCK) (Borikova et al., 2010). This causes actin stress fiber formation, which compromises the integrity of cell-cell junctions. Although *CCM1* is the most commonly mutated gene, mutations in *CCM3* cause the earliest onset and most aggressive form of this disease (Shenkar et al., 2015).

A possible reason for the enhanced aggressiveness associated with *CCM3* mutations may be that it functions in multiple complexes concurrently. Along with the hetero-trimeric CCM complex, CCM3 is also present in the STRIPAK complex (Kean et al., 2011). This complex contains a striatin backbone to which CCM3 binds and provides both phosphorylation and de-phosphorylation activity through germinal center kinase class III (GCKIII) kinases (MST3, MST4, and MST20) and protein phosphatase 2 (PP2A/C), respectively (Kean et al., 2011). Also bound to striatin is the MOB kinase activator (MOB3) and the striatin-interacting proteins (STRIP1/2), which themselves tether a number of proteins, including the sarcolemma-associated protein (SLMAP), IKK kinase suppressor (SIKE), and cortactin-binding protein (CTTNBP2) (Kean et al., 2011). STRIPAK has been implicated in a number of human diseases (Hwang and Pallas, 2014) and uses CCM3 as a kinase adaptor (Ceccarelli et al., 2011). CCM/GCKIII activity affects Golgi localization (Kean et al., 2011) and cytoskeletal organization by directing

This is an open access article under the CC BY license (http://creativecommons.org/licenses/by/4.0/).

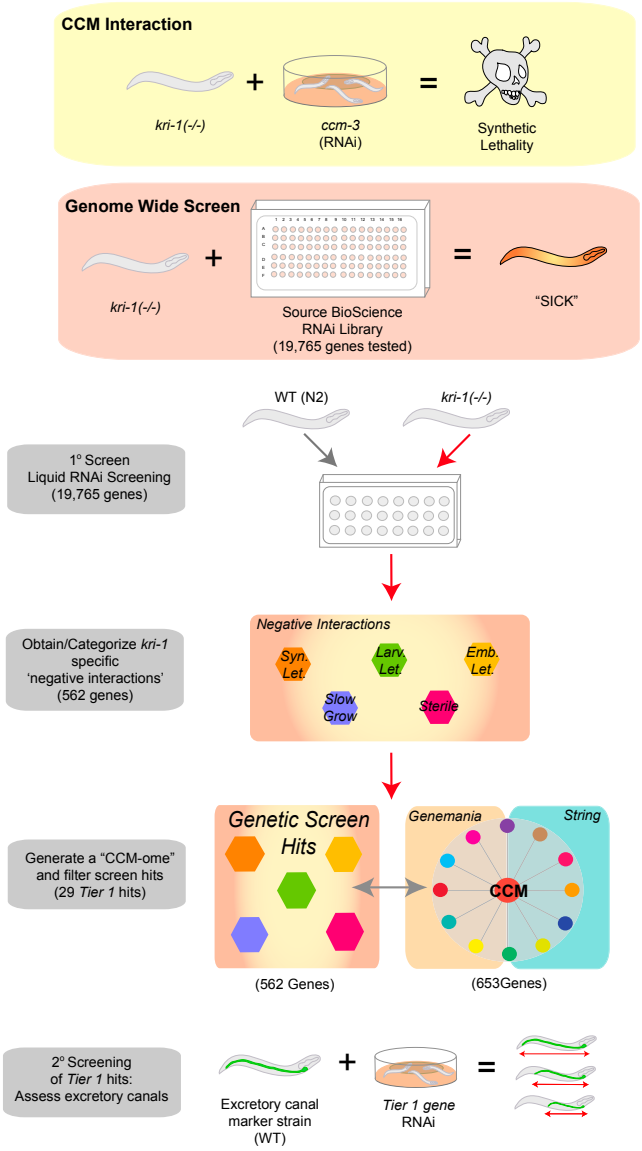

Figure 1. Flowchart of Genome-wide RNAi Screen

Taking advantage of the synthetic lethal interaction previously identified between *kri-1*/CCM1 and *ccm-3*/CCM3 (Lant et al., 2015), 562 genes were identified that exhibit negative interactions (Emb. Let., embryonic lethality, sterility, or slow growth; Larv. Let., larval lethality; Syn. Let., synthetic lethality) when ablated by RNAi in *kri-1* mutants. In parallel, a phenolog-like approach using GeneMANIA and STRING was used to generate a "CCM-ome" from genes known to function in human CCM signaling pathways. The 29 overlapping genes between these two sets ("tier 1 hits") were assessed for *ccm-3* phenotypes in *C. elegans*, such as excretory canal truncations. See also Figure S1.

the phosphorylation of a number of substrates, such as the actin-binding protein moesin (Zheng et al., 2010). Furthermore, emerging evidence indicates that CCM3 is able to act independently of the other two CCM proteins (Lant et al., 2015; Yoruk et al., 2012; You et al., 2017; Zhou et al., 2016a).

Although there have been intense efforts to understand the mechanisms by which CCM1 and CCM2 regulate vascular integrity, much less is known about the role of CCM3. Our aim in this study was to interrogate the *C. elegans ccm-3* network by first conducting a whole-genome RNAi screen to identify a comprehensive set of genes that exhibit similar synthetic lethal interactions with *kri-1/CCM1* as *ccm-3* (Figure 1). Large-scale reverse genetics screens in *C. elegans* have many advantages for understanding poorly characterized genes, which often provide important insights into the biological functions of genes implicated in human diseases (Meier et al., 2014; Silverman et al., 2009; Sin et al., 2014). We uncovered more than 500 genes that exhibited strong negative genetic interactions with *kri-1* and function in a range of cellular processes, including vesicle trafficking and cytoskeletal dynamics. By using a phenolog-like approach (McGary et al., 2010), we cross-referenced these *C. elegans* genes with a network assembled from genes previously shown to function in human CCM signaling. The resultant 29 genes (tier 1 hits) were systematically knocked down by RNAi and evaluated for *ccm-3*-specific phenotypes, such as excretory canal truncations. Of the 29 tier 1 genes, 14 caused strong excretory canal truncations and membrane defects when knocked down in wild-type animals. The most severe canal defects were caused by ablation of *mop-25.2*, a homolog of mouse embryo scaffolding protein 25 (MO25), which is involved in mediating AMPK signaling (Boudeau et al., 2003, 2004). Our analysis reveals a role for MOP-25.2, independent of its canonical binding partners, in the localization of both CCM-3 and GCK-1 to apical membranes necessary for biological tube integrity. Finally, we show that loss of *MO25* phenocopies *CCM3* ablation in endothelial cells by causing actin stress fiber formation. The combination of unbiased screening and bioinformatics analysis in *C. elegans* affords a powerful and efficient method for understanding how CCM proteins regulate biological tube development and may even uncover therapeutic targets.

RESULTS

Whole-Genome Screen to Identify Genes in the *ccm-3* Pathway

We previously observed that, although loss of neither *kri-1* nor *ccm-3* on its own affects the survival of the worm, ablation of *ccm-3* in *kri-1* mutants results in synthetic lethality (Lant et al., 2015). We reasoned that other genes that cause similar negative genetic interactions with *kri-1* may act in the *ccm-3* pathway or cooperate with its *in vivo* functions. Therefore, we conducted a full-genome RNAi screen using the Source BioScience RNAi Library, which covers ~96% of annotated genes in the *C. elegans* genome, and identified 562 genes that reduced fitness of *kri-1* mutants but not wild-type worms (Figure 1). These phenotypes, which include lethality at all stages of development, slow growth, and reduced fertility, all represent negative genetic interactions (Figure S1). Using the GeneMANIA application in Cytoscape, we constructed a network on the basis of these interactions to evaluate connectivity between our screen hits and genes known to be involved in CCM signaling (Figures S1 and S2, blue circles). Of the 562 genes identified, 237 had annotated interactions (genetic, physical, and/or predicted) with one another, while the remaining 325 "orphan" genes had only genetic interactions with *kri-1* (Figure S1). For this study we focused on the 237 genes

Figure 2. *C. elegans* CCM Network Map

The network, with gene clusters showing enrichments in specific signaling pathways and cellular processes, was constructed using the GeneMANIA app in Cytoscape and gene annotations from Wormbase (www.wormbase.org). Genetic, physical, and predicted interactions are marked with green, pink, and orange lines, respectively. Negative hits from the primary screen are shown to have interaction with the CCM-related genes (blue spheres). Hits that will later be identified as "tier 1" are indicated by triangular outline.
See also Tables S1 and S4 and Figure S2.

with documented interactions. Using Gene Ontology (GO) classification, these genes were found to be associated with a number of cellular processes, with a notable enrichment in cell localization and migration categories (including cell migration, cell motility, localization of the cell, and inductive cell migration) (Figure S2). Analysis of their functional roles indicate that a number fall into well-defined signaling cascades or cell process categories (Figure 2; Table S1). For example, we identified several cytoskeletal genes (i.e., actin, tubulin, interfilament organizer, and chaperones) and genes involved in small G protein signaling (i.e., small GTPases, GEF, and RHO-activating proteins). This is in line with previously described roles of CCM proteins in the regulation of actin polymerization and cell junction stability through Rho signaling (Borikova et al., 2010; Stockton et al., 2010; Whitehead et al., 2009). Consistent with observations in mammalian systems (Draheim et al., 2015; Zhou et al., 2015, 2016b) we also identified a number of MAPK signaling genes, such as a MEKK3 kinase, MAPK phosphatases, and a KLF transcription factor. Finally, several vesicle-trafficking proteins (including the exocyst complex, endosome-associated GTPase, and components of the adaptin complex) were identified, consistent with our recent observations on CCM-3/STRIPAK function in biological tube development (Lant et al., 2015; Pal et al., 2017).

To refine the primary network into a set of genes that are evolutionarily conserved, we used a "phenolog"-like approach (McGary et al., 2010). We reasoned that filtering the primary screen hits to identify nematode genes with human homologs would enrich for genes relevant to CCM biology. We selected 35 genes (Table S4) previously shown to function in human CCM signaling (Borikova et al., 2010; Fischer et al., 2013; Glading and Ginsberg, 2010; Storkebaum et al., 2011; Zhang et al., 2013a) to generate a predicted "CCM-ome." This CCM-ome gene list, generated using GeneMANIA and STRING algorithms, was converted to their nematode orthologs, yielding 653 genes (see STAR Methods for more details). Comparing this list with the 562 genes identified from the unbiased RNAi screen revealed 29 genes in common, which we refer to as "tier 1" hits (Figure 2, triangles, and Figure 3A; Table 1). We reasoned that genes identified in the RNAi screen that are orthologous to human genes in the CCM-ome would predict roles in CCM3 biology.

To investigate their *in vivo* functions, we used the *C. elegans* excretory canal as a model. This unicellular tube extends bi-directionally along both sides of the worm and functions as a renal system for the animal (Nelson and Riddle, 1984) (Figure 3B). Loss of *ccm-3* causes significant truncations and "cyst" formation in excretory canals (Lant et al., 2015). We systematically ablated the 29 tier 1 genes by RNAi in wild-type animals and quantified excretory canal lengths. This was compared with a list of 29 randomly selected "control set" genes (Table S2). We found that the tier 1 set was significantly enriched ($p = 6.9 \times 10^{-36}$) for genes that caused canal truncations compared with the control set (Figures 3C, S3A, and S3B). Using the distribution of canal lengths under control conditions (Figure 3B), we denote "truncations" as canals that are <80% the length of those in wild-type animals. For a gene to cause a biologically relevant truncation when ablated, it must cause at least 5 times more canal truncations in the population of worms compared with control RNAi; a population of worms on control RNAi exhibits ~7% truncation (33 of 500), so for a gene to cause truncation, ≥35% of animals must have truncated canals. We defined a strong truncation to be similar to *ccm-3* mutants (≥80% of animals with truncated canals). Analysis of individual genes within

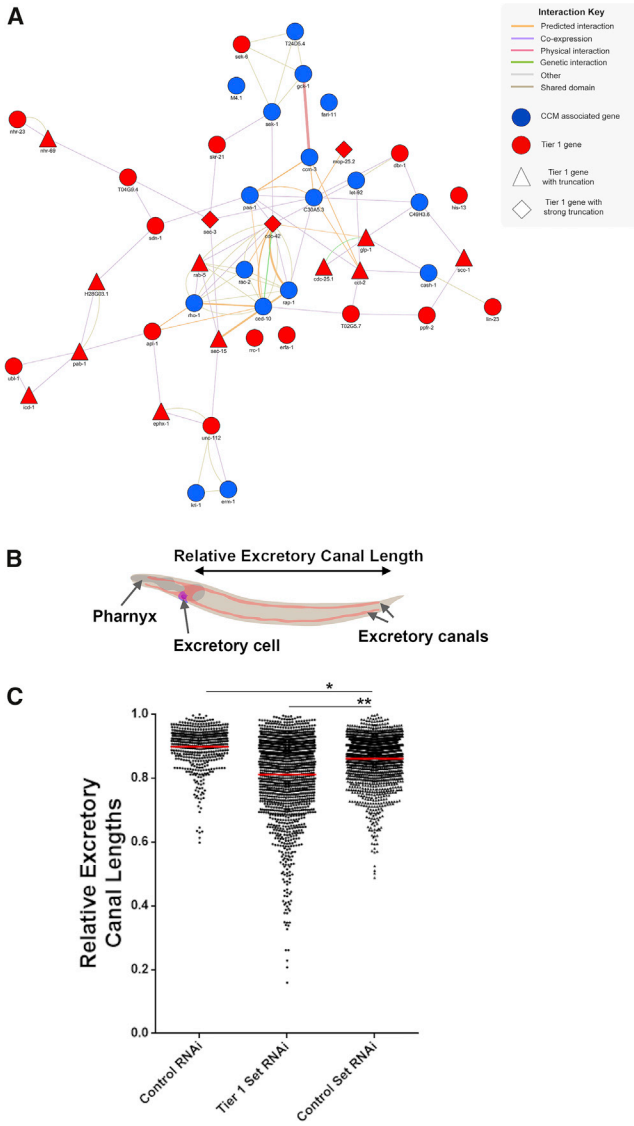

Figure 3. Effect of Tier 1 Genes on Excretory Canal Lengths

(A) Genes classified as tier 1 hits (red) form a highly interactive network with CCM-associated genes (blue). Tier 1 hits were secondarily analyzed for the *ccm-3*-mutant phenotype, excretory canal truncation.

(B) Worm canals were measured as a ratio of canal length to body length.

(C) Quantitation of canal truncations shows that tier 1 hits produced significantly more truncated canals than wild-type canals (n = 1,450; * and **$p < 0.05$), and a randomly generated "control set" of genes. Analysis of individual tier 1 hits (Table 1) also indicated genes that caused truncations (triangle) and strong truncations (diamond) when ablated.

See also Table S2 and Figure S3.

each set (Figures S3A and S3B; Tables 1 and S2) revealed that the control set had 26 genes with no truncation, 3 genes causing truncation, and no genes causing strong truncation. Conversely, the tier 1 set contained only 15 genes with no truncation, 11 genes causing truncations, and 3 genes causing strong truncations, which was a significant enrichment in genes required for canal extension compared with the control set ($p = 0.0031$). Tier 1 genes causing canal truncations (Figure 3A, triangle- and diamond-outlined genes) represent a range of cellular processes, such as *rab-5* (early endosome targeting GTPase), the Rho GEF ortholog *ephx-1*, the small GTPase *cdc-42*, and *sec-3/sec-15* (exocyst). We also identified a number of genes that have no previously documented roles in excretory canal morphology, including the chaperonin complex subunit *cct-2*, the RNA lariat debranching enzyme *dbr-1*, polyadenylate-binding protein *pab-1*, and Rad21/Rec8-like cohesion protein *scc-1*. In addition, two uncharacterized genes, the RBM (RNA binding motif-containing) ortholog *H28G03.1* and nuclear hormone receptor *nhr-69*, also caused canal truncations when ablated.

Genes with *CCM1/kri-1* Phenotypes

Because the methodology of both the RNAi screen and the subsequent bioinformatic filtering do not bias against potential *CCM1/kri-1* interactors, we asked whether any of the tier 1 hits would also cause *kri-1* phenotypes. Loss of *kri-1* causes resistance to ionizing radiation (IR)-induced germline apoptosis in the pachytene region (Ito et al., 2010) (Figure S3C, yellow asterisks). Conversely, loss of *ccm-3* causes oocyte growth defects that leads to their death in the distal end of the germline (Figure S3D, red asterisk). We quantified germ cell corpses after ablating tier 1 genes by RNAi in wild-type worms exposed to 60 Gy of IR, using *kri-1* and the anti-apoptotic Bcl-2 homolog *ced-9* as controls. Although ablation of some genes (*cct-2*, *cdc-25.1*, *cdc-42*, *erfa-1*, *T04G9.4*, *ubl-1*, and *unc-112*) caused germline defects that made it impossible to quantify apoptotic corpses, five genes (Figure S3E; *dbr-1*, *his-13*, *icd-1*, *lin-23*, and *nhr-23*) caused suppression of apoptosis similar to *kri-1* RNAi ($n = 50$, $p < 0.05$ from control RNAi, $p > 0.05$ from *kri-1* RNAi). If we define suppression as less than or equal to the levels of physiological apoptosis, or two corpses per gonad arm (Gumienny et al., 1999), ablation of *kri-1* by RNAi caused ~50% suppression of apoptosis (24 of 50 germline arms with two or fewer corpses). Only *his-13* RNAi caused a greater suppression of apoptosis (29 of 50 germline arms) than *kri-1*.

mop-25.2 Is Required for Excretory Canal Integrity

Of the tier 1 hits (Figure S3A), knockdown of MO25 ortholog *mop-25.2* caused the most severe canal truncations (50 of 50 canals with canals <80% wild-type length) that were even more severe than knockdown of *ccm-3* or *gck-1* ($p < 0.05$ in both cases) (Figures 4A and 4B). Consistent with loss of *ccm-3* (Lant et al., 2015), we frequently observed distended lumen and distal canal tip cysts in animals depleted of *mop-25.2* (Figure 4C, middle and bottom). Interestingly, RNAi to either *gck-1* or *mop-25.2* significantly exacerbated truncations in *ccm-3* mutants ($p = 1.089 \times 10^{-9}$ and $p = 2.49 \times 10^{-5}$, respectively) (Figure 4D). We also observed this with *gck-1* mutant worms, in which depletion of *ccm-3* or *mop-25.2* significantly enhanced canal truncations ($p = 3.30 \times 10^{-09}$, and $p = 8.68 \times 10^{-08}$, respectively) (Figure 4D). Previously, we found that loss of *ccm-3* and STRIPAK genes affected the stability of Golgi as well as subcellular localization of CDC-42 and the endocytic recycling protein RAB-11 in the canal. Knockdown of *mop-25.2* also diminished puncta for these

Table 1. Tier 1 Hits and Their Human Homologs

Gene Name	WB Gene ID	Truncation Rating	Human Gene Homolog	Human Gene ID
apl-1	WBGene00000149	no truncation	APLP1	ENSG00000105290
cct-2	WBGene00000378	truncation	CCT2	ENSG00000166226
cdc-25.1	WBGene00000386	truncation	CDC25A	ENSG00000164045
cdc-42	WBGene00000390	strong truncation	CDC42	ENSG00000070831
dbr-1	WBGene00000937	no truncation	DBR1	ENSG00000138231
ephx-1	WBGene00019487	truncation	ARHGEF16	ENSG00000130762
erfa-1	WBGene00020269	no truncation	ETF1	ENSG00000120705
glp-1	WBGene00001609	truncation	NOTCH2	ENSG00000134250
H28G03.1	WBGene00019249	truncation	HNRNPA1	ENSG00000135486
his-13	WBGene00001887	no truncation	HIST2H3D	ENSG00000183598
icd-1	WBGene00002045	truncation	BTF3	ENSG00000145741
lin-23	WBGene00003009	no truncation	FBXW11	ENSG00000072803
mop-25.2	WBGene00013140	strong truncation	CAB39	ENSG00000135932
nhr-23	WBGene00003622	no truncation	RORA	ENSG00000069667
nhr-69	WBGene00003659	truncation	HNF4A	ENSG00000101076
pab-1	WBGene00003902	truncation	PABPC4	ENSG00000090621
ppfr-2	WBGene00017064	no truncation	PPP4R2	ENSG00000163605
rab-5	WBGene00004268	truncation	RAB5B	ENSG00000111540
rrc-1	WBGene00009800	no truncation	ARHGAP30	ENSG00000186517
scc-1	WBGene00004737	truncation	RAD21	ENSG00000164754
sdn-1	WBGene00004749	no truncation	SDC1	ENSG00000115884
sec-15	WBGene00016188	truncation	EXOC6	ENSG00000138190
sec-3	WBGene00018703	strong truncation	EXOC1	ENSG00000090989
sek-6	WBGene00012162	no truncation	MAP2K4	ENSG00000065559
skr-21	WBGene00004827	no truncation	SKP1	ENSG00000113558
T02G5.7	WBGene00020166	no truncation	ACAT1	ENSG00000075239
T04G9.4	WBGene00020215	no truncation	AASDHPPT	ENSG00000149313
ubl-1	WBGene00006725	no truncation	RPS27A	ENSG00000143947
unc-112	WBGene00006836	no truncation	FERMT2	ENSG00000073712

Many *C. elegans* genes are the single homologs for multiple human genes or gene isoforms. Listed above are the human homologs on the basis of the BLASTP matches per Wormbase.org. For an expanded list of possible human homologs, see Table S4.

markers (Figure 4E; Table S3), indicating a similar role as CCM-3/STRIPAK. Collectively, these results reveal a role for MOP-25.2 in canal extension by both CCM-3/GCK-1-dependent and CCM-3/GCK-1-independent mechanisms.

Because there are three nematode MO25 paralogs in *C. elegans*, in which *mop-25.1* and *mop-25.3* are more distantly related to *mop-25.2* (Chien et al., 2013), we wondered if they shared similar roles in canal development. Ablation of *mop-25.1* and *mop-25.3* caused weak canal truncations (Figure S4) and diminished puncta of CDC-42/recycling markers (Table S3), which concurs with previous studies showing some overlapping functions (Chien et al., 2013; Denning et al., 2012). Because MO25 regulates AMPK signaling through the MO25/STRAD/LKB1 complex (Boudeau et al., 2004; Hawley et al., 2003), we wondered whether MOP-25.2 regulates canal extension through the AMPK homolog. Therefore, we ablated both homologs of the catalytic alpha subunit of AMPK (*aak-1/aak-2*), the upstream LKB1 homolog (*par-4*), the ortholog of STRAD (*strd-1*), and the STRD-1 associated kinase (*sad-1*). Only knockdown of *par-4* caused mild canal truncations (Figure S5), suggesting an alternate function for MOP-25.2 in canal extension that is distinct from its canonical binding partners.

mop-25.2 Is Required for Germline Rachis Stability

Loss of *ccm-3* also causes sterility, whereby the germline lumen (rachis) collapses and impairs oocyte growth (Pal et al., 2017) (Figures 4F and 4G). Previously, *mop-25.2* was shown to be required for embryonic development, whereby the *mop-25.2(ok2073)* deletion allele caused a maternal lethal effect (Chien et al., 2013), so we wondered if *mop-25.2* shared any germline phenotypes with *ccm-3*. Using markers for both germline nuclei (mCherry::HIS-58) and membranes (GFP::PH [PLCdelta1]), knockdown of *mop-25.2* caused rachis membrane collapse (Figure 4H, yellow asterisk) and small and rounded oocytes (Figure 4H, blue asterisk) in approximately 60% of animals (31 of 50). These germline defects were strikingly similar to those caused by loss of *ccm-3*, providing further support for MOP-25.2 playing a key role in the biological functions of CCM-3/STRIPAK.

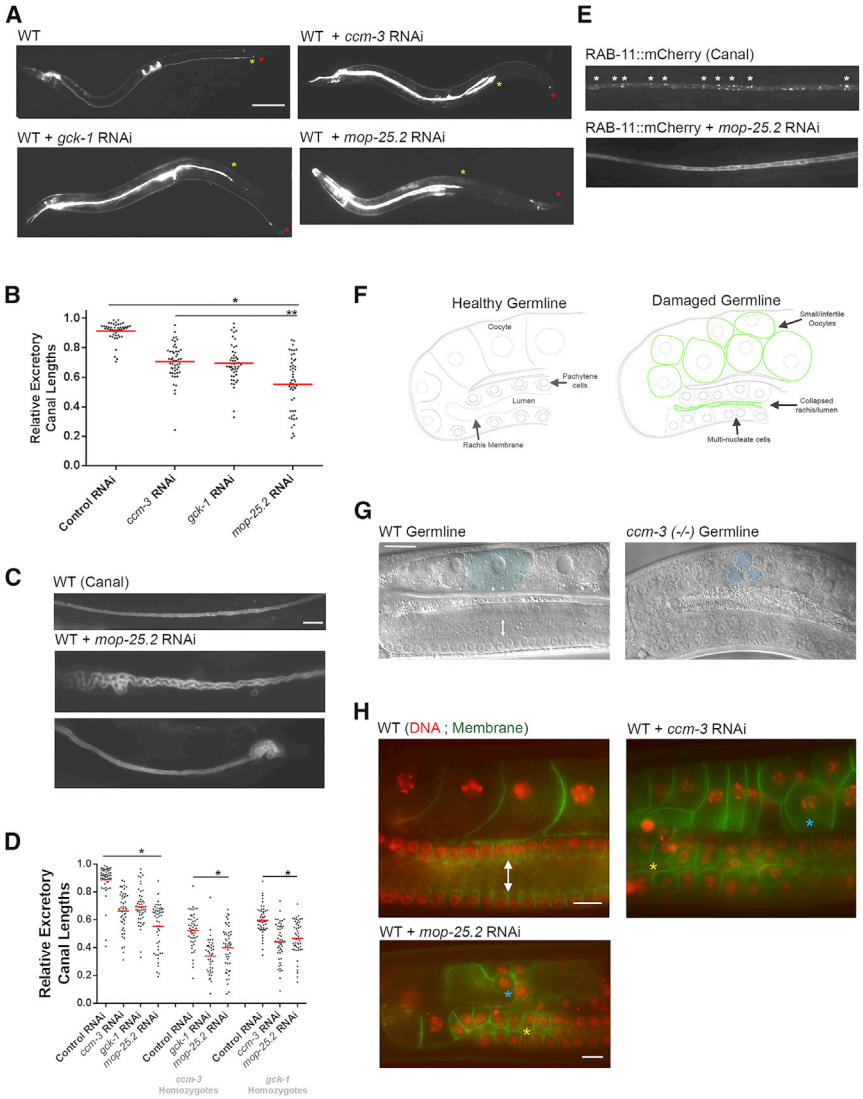

Figure 4. *mop-25.2* Is Required for Excretory Canal Extension and Germline Integrity

(A and B) (A) Knockdown of *ccm-3*, *gck-1*, and *mop-25.2* causes significant canal truncations (B) (n = 50, *p < 0.05), with *mop-25.2* significantly more truncated than either (**p < 0.05). The red asterisk denotes the distal worm measurement, and the yellow asterisk indicates the end of the canal.

(C) Compared with wild-type (WT) canals, *mop-25.2* RNAi causes lumen defects and distal tip cysts.

(D) Loss of either *gck-1* or *mop-25.2* in a *ccm-3*-mutant background exacerbates canal truncations, and similarly, loss of *ccm-3* or *mop-25.2* in a *gck-1*-mutant background causes more severe truncations (all n = 50, *p < 0.05).

(E) Ablation of *mop-25.2* reduces endocytic recycling markers from the distal region of the canal (see Table S3).

(F) Cartoon illustrating a healthy (wild-type) *C. elegans* germline and a *ccm-3* mutant with a damaged germline.

(G) In *ccm-3* mutants, the lumen bordered by the rachis membrane collapses (white arrow), resulting in underdeveloped oocytes (blue overlays).

(H) Using fluorescent membrane and nuclear markers (GFP::PH [PLC1delta1], mCherry::his-58) to visualize the germline, knockdown of *mop-25.2* phenocopies *ccm-3* mutants. Rachis collapse (yellow asterisks) and small oocytes (blue asterisks) was observed in ~60% of worms treated with *mop-25.2* RNAi (n = 50).

Scale bars, 50 μm (A) and 10 μm (C, E, G, H). See also Table S3 and Figures S4 and S5.

mop-25.2 Is Required for CCM-3 Localization

Previously, we showed that ablation of *gck-1* in the germline caused CCM-3 to relocalize from the apical membrane to meiotic nuclei (Pal et al., 2017). Because mammalian MO25 has been shown to bind and stabilize GCKIII class kinases (Filippi et al., 2011), and a MO25-GCKIII-CCM3 ternary complex may exist (Yin et al., 2012), we asked if MOP-25.2 affects CCM-3 localization in a manner similar to GCK-1. CCM-3 localizes to apical membranes in both the canal and germline (Lant et al., 2015; Pal et al., 2017) (Figures 5A and 5B, top). Using GFP translational reporters for CCM-3, we measured the fluorescence of GFP::CCM-3 in the excretory canal (along the lumen) and the pachytene region of the germline. Knockdown of *ccm-3* caused the expected dissipation of canal GFP::CCM-3 (Figure 5A), and loss of *gck-1* did not significantly diminish GFP signal compared with controls (Figure 5A, fourth panel, and Figure 5C; p = 0.58), but it did cause punctate patches (yellow asterisk) of CCM-3 along canals. This punctate CCM-3 localization was observed in 12% of wild-type canals (n = 50), but ablation of *gck-1* significantly increased this to 46% (p = 0.00014). Loss of *mop-25.2*, on the other hand, significantly decreased CCM-3 signal in the canal ($p = 6.74 \times 10^{-10}$), although not to the same extent as *ccm-3* knockdown (Figure 5A, fifth panel, and Figure 5C). Canals of worms treated with *mop-25.2* RNAi did not have significantly increased levels of punctate CCM-3 compared with wild-type (p = 0.41). Similar effects were observed in the germline. GFP::CCM-3 signal is on the luminal membrane of the rachis (Figure 5B, yellow arrow/asterisk) above the pachytene cells (Figure 5B, red asterisk). Where knockdown of *ccm-3* ablated the GFP signal (Figure 5B, second panels), as observed before, loss of *gck-1* caused CCM-3 relocalization into pachytene nuclei (Figure 5B, third panels). However, loss of *mop-25.2* significantly diminished GFP::CCM-3 signal on the lumen (Figure 5B, fourth panel, and Figure 5D; $p = 1.02 \times 10^{-13}$) but did not cause its relocalization to nuclei. Thus, although *gck-1* and *mop-25.2* both cause identical defects when ablated, they differentially affect CCM-3 localization in both the excretory canal and germline.

mop-25.2 Is Required for GCK-1 Localization

Because *mop-25.2* knockdown dramatically affected CCM-3 localization, we next asked if it had a similar effect on GCK-1.

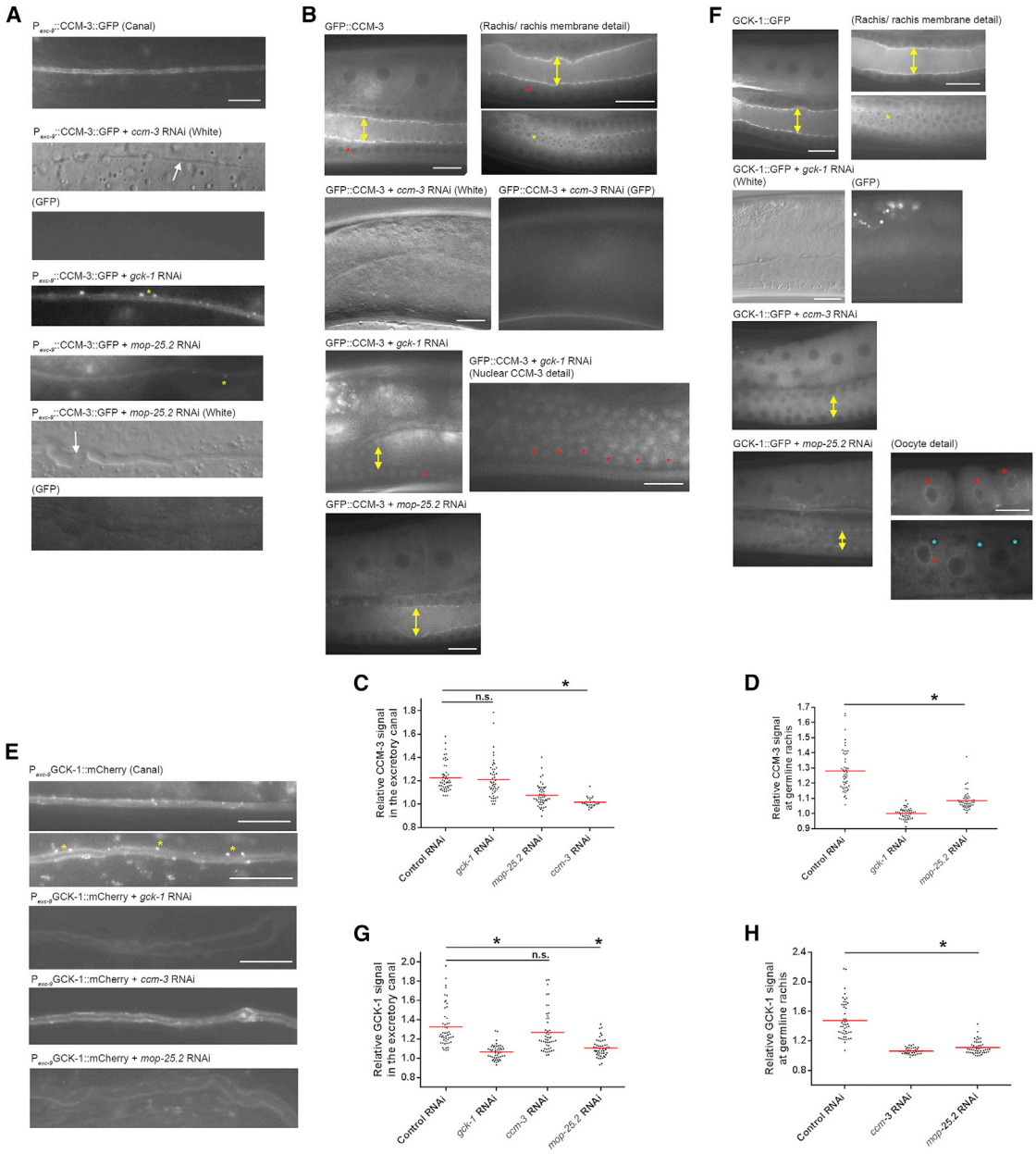

Figure 5. *mop-25.2* Is Required for Membrane Localization of CCM-3 and GCK-1

(A, B, E, and F, top panels) Both CCM-3 and GCK-1 localize to apical membranes of the excretory canal and germline.

(A) *ccm-3* RNAi diminishes GFP::CCM-3 signal in excretory canals as expected (C; n = 50, *p < 0.05), whereas knockdown of *gck-1* causes CCM-3 to relocalize into discrete puncta along the apical membrane (yellow asterisk). Knockdown of *mop-25.2* diminishes CCM-3 signal significantly (n = 50, *p < 0.05).

(B) GFP::CCM-3 localizes to rachis membrane in the germline (yellow arrow) around openings to the rachis (yellow asterisk) but not within the cell nuclei themselves (red asterisks).

(C) *ccm-3* RNAi diminishes GFP::CCM-3 signal in excretory canals as expected (n = 50, *p < 0.05), whereas knockdown of *gck-1* causes CCM-3 to relocalize into discrete puncta along the apical membrane (yellow asterisk). Knockdown of *mop-25.2* diminishes CCM-3 signal significantly (n = 50, *p < 0.05).

(D) Depletion of *gck-1* causes GFP::CCM-3 relocalization to germ cell nuclei, whereas *mop-25.2* RNAi reduced its levels on the rachis membrane (n = 50, *p < 0.05).

(E) GCK-1 in the canal is frequently punctate (yellow asterisks).

(F) In the germline, *gck-1* RNAi completely ablates GFP::GCK-1 signal.

(G) Ablation of *gck-1* or *mop-25.2* reduced GFP::GCK-1 signal (n = 50, *p < 0.05), but knockdown of *ccm-3* did not (see E), although it reduced punctate localization by half (n = 50, p < 0.05).

(H) Depletion of *ccm-3* or *mop-25.2* significantly reduced GFP::GCK-1 membrane localization (n = 50, *p < 0.05). *mop-25.2* RNAi also caused perinuclear accumulation of GCK-1 (red asterisks) and patchy cytoplasmic localization of GFP::GCK-1 in oocytes (blue asterisks).

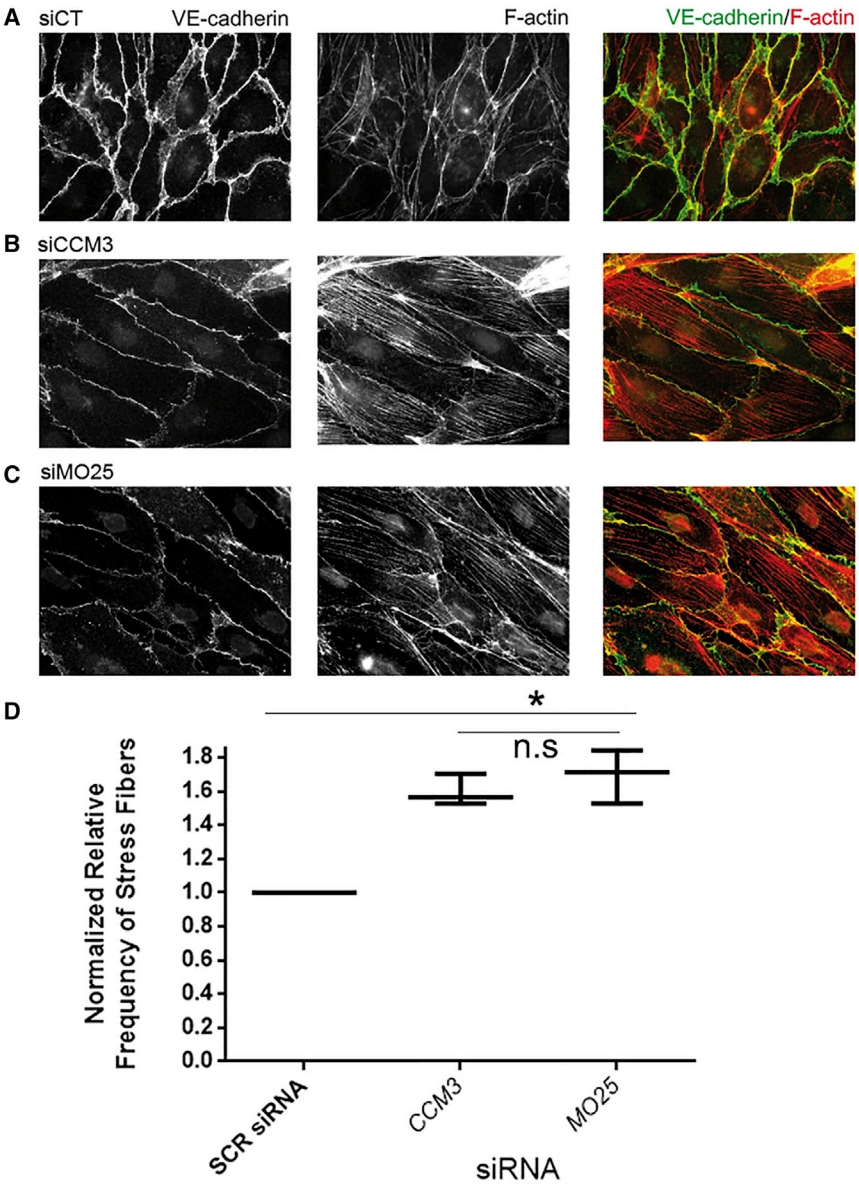

Figure 6. Loss of MO25 Causes Stress Fiber Formation in Endothelial Cells

(A–D) Pooled HUVECs transfected with control siRNA (A), siCCM3 (B), and siMO25 (C) and incubated with antibodies against VE-cadherin and phalloidin (F-actin) were quantified for the formation of transverse actin fibers (SFs) (D). Loss of both CCM3 and MO25 caused a significant increase in stress fiber formation (n = 3 independent experiments, *$p < 0.05$).

GCK-1 co-localizes in a punctate manner with CCM-3 along the apical membrane of the canal (Figure 5E, yellow asterisks) and the rachis membrane of the germline (Figure 5F, yellow arrow/asterisk). Ablation of *gck-1*, as expected, caused signal to disappear in both tissues (Figures 5E and 5F, second panels, and Figures 5G and 5H). In the canals, ablation of *ccm-3* did not change either GCK-1::mCherry localization or its fluorescence intensity ($p = 0.18$) (Figure 5E, third panel, and Figure 5G), but it did reduce the punctate distribution of GCK-1 to ~30% (16 of 50, $p = 0.0086$). Similarly, in the germline, loss of *ccm-3* did not cause relocalization of GCK-1 but significantly diminished its signal ($p = 4.35 \times 10^{-16}$) along the rachis membrane (Figure 5F, third panel, and Figure 5H). As with GFP::CCM-3, knockdown of *mop-25.2* caused a significant reduction of GCK-1 signal in the apical membranes of both the canal and germline ($p = 5.11 \times 10^{-09}$ and $p = 3.24 \times 10^{-14}$, respectively) (Figures 5E and 5F, fourth panels, and Figures 5G and 5H). Interestingly, ablation of *mop-25.2* also reduced the punctate localization of GCK-1::mCherry ($p = 0.0022$) in the canal and increased its perinuclear and patchy cytoplasmic localization in oocytes ($p = 0.00028$) (Figure 5F, fourth panel insets, red and blue asterisks, respectively). Thus, MOP-25.2 regulates the integrity of the excretory canal and germline, most likely by controlling the localization of CCM-3 and GCK-1.

Knockdown of CCM3 and MO25 Causes Stress Fibers in Endothelial Cells

In order to assess if the role of *mop-25.2* is conserved, we ablated both CCM3 and MO25 in human umbilical vein endothelial cells (HUVECs) and assessed stress fiber (SF) formation. Loss of CCM proteins cause actin stress fibers through increased RhoA/ROCK activity (Richardson et al., 2013; Stockton et al., 2010). Staining for both VE-cadherin and F-actin, we observe the change in dynamics between the two (Abu Taha and Schnittler, 2014). With control scrambled (SCR) small interfering RNA (siRNA), VE-cadherin and F-actin largely co-localize at cell junctions (Figures 6A–6C). However, siRNA to both CCM3 and MO25 lock the actin into transversal arcs that cross the nucleus and stretch across the cell (Tojkander et al., 2012). Prevalence of stress fibers in cell populations (Figure 6D) showed significant increases with siRNA to CCM3 and MO25 ($p = 0.0083$ and $p = 0.018$, respectively, $n > 300$), indicating that loss of MO25 phenocopies loss of CCM3 in endothelial cells.

DISCUSSION

Here, we took advantage of the genetic tools of *C. elegans* to interrogate the CCM gene network, focusing on the less studied *CCM3* branch. Our RNAi screen identified 562 genes that cause negative genetic interactions in *kri-1/CCM1* mutants, similar to

ablation of *ccm-3*. Although we focused on the 237 genes with annotated interactions, greater data integration of the "orphan genes" in the future should provide more insights into their gene-gene interactions and biological functions. Many of the genes with well-documented interactions clustered into a limited but functionally diverse number of biological processes, including protein translation, cytoskeletal dynamics, and vesicle trafficking (Figure 2; Table S1). This is consistent with our previous work showing a role for CCM3 in these processes to control biological tube integrity (Lant et al., 2015; Pal et al., 2017). Our screen uncovered several expected hits, including genes encoding small GTPases, Notch, MAPK, and KLF (Table S1), confirming the robustness of this method (Borikova et al., 2010; Ma et al., 2007; You et al., 2013; Zhou et al., 2015). The identification of cell cycle, histone, and ion channel genes (Figure 2; Table S1), expands the number of biological processes affected by CCM signaling, which will be interesting to investigate in the future.

We were particularly interested in characterizing the functions of genes that are conserved in humans. Using the bioinformatics platforms GeneMANIA and STRING (von Mering et al., 2005; Mostafavi et al., 2008) to generate a human CCM-ome allowed us to interrogate a limited set of genes predicted to have conserved functions in CCM biology. Remarkably, of the 29 tier 1 genes, 14 caused significant excretory canal truncations when ablated. Genes that regulate canal integrity are uncommon (Buechner et al., 1999; Sundaram and Buechner, 2016), and of these 14 genes, 3 were previously known to affect the excretory canal: *glp-1* (Abdus-Saboor et al., 2011), *rab-5* (Mattingly and Buechner, 2011), and *cdc-42* (Lant et al., 2015). The remaining 11 genes exhibit previously undocumented excretory cell phenotypes. Because the tier 1 genes might also function in the KRI-1/CCM1 pathway, we evaluated their role in germline apoptosis and found that 5 genes (Figure S3E) conferred resistance to radiation-induced germline apoptosis when ablated, similar to *kri-1*. Although this is not as striking as the frequency of genes that affect the excretory canal, it is possible that we have uncovered some genes in which the CCM-3 and KRI-1 pathways converge. Only ablation of *his-13*, exceeded "*kri-1*-level" apoptosis suppression, and while *his-13* has not been reported to affect IR-induced germline apoptosis, histones affect the expression of many genes, so it will be interesting to determine if *his-13* has a direct role in CCM signaling.

Tier 1 genes causing *ccm-3*-like canal truncations included a number of small GTPases and small GTPase regulators, which is not surprising given that RhoA is hyper-activated in the absence of CCM proteins (Richardson et al., 2013; Stockton et al., 2010). We previously reported that CCM-3 regulates another small GTPase, CDC-42 (Lant et al., 2015), which was also identified as a tier 1 hit in this study (Figure S3; Table 1). In addition, we identify a number of GTPase related genes (Figure 2), including the Rho GEF *ephx-1*, which has been reported to regulate CDC-42 activity in both nematodes and human cells (Oliver et al., 2011; Walck-Shannon et al., 2016). Therefore, we predict that a more extensive network of small GTPases are involved in CCM signaling.

Consistent with our previous work showing that CCM-3/STRIPAK regulates endocytic recycling (Lant et al., 2015; Pal et al., 2017), several tier 1 genes encode vesicle-trafficking proteins, including the early endosomal GTPase *rab-5* and exocyst complex genes *sec-3* and *sec-15*. This is significant because we previously discovered a link between CCM-3 and the exocyst complex gene *exoc-8* (Lant et al., 2015), which was also identified in the RNAi screen. Work by Armenti et al. (2014) identified important roles for the exocyst gene *sec-5* and the exocyst complex regulator *ral-1* in excretory canal development, with localization of exocyst proteins to apical membrane mediated by polarity proteins. Combined, our work showing that CCM-3 is required for proper localization of the polarity proteins PAR-2 and PAR-6 (Pal et al., 2017) suggests that CCM-3 may coordinate polarity establishment and endocytic trafficking during biological tube development.

Many of the tier 1 genes had not been previously implicated in functions related to CCM-3/CCM3 signaling, and of these, the most intriguing gene to us was the MO25/CAB39 homolog *mop-25.2*. Not only did its ablation cause the strongest canal truncations, but it also had similar germline defects as observed in *ccm-3* and *gck-1* mutants (small oocytes and rachis collapse) (Figure 4). Although *mop-25.2* is required for localization of CCM-3 to apical membranes, its co-ablation with *ccm-3* or *gck-1* caused additive effects on canal truncations (Figure 4D). We propose that MOP-25.2 functions to integrate CCM-3/GCK-1, and likely other factors, to promote canal extension and germline integrity. Although mammalian MO25 is best known to regulate AMPK signaling, its role in *C. elegans* tubulogenesis is independent of its canonical binding partners LKB1/STRAD and AMPK (Figure S5). Canal defects caused by knockdown of *par-4* and *mop-25.2*, but not *strd-1* and the AMPK genes, are interesting in light of observations showing that *par-4* and *strd-1* function independently of their canonical pathway (Narbonne and Roy, 2009; Narbonne et al., 2010).

The impact of losing *mop-25.2* on CCM-3 localization at the canal lumen and germline rachis is distinct from *gck-1* loss, which caused CCM-3 to localize into discrete puncta in the canal (Figure 5A) and nuclei of the meiotic germline (Figure 5B) (Pal et al., 2017). Interfering with binding to GCK-1 causes CCM-3 to relocalize to the nucleus, whereas loss of binding to CASH-1 (striatin) disrupts apical membrane localization but not nuclear relocalization (Pal et al., 2017). Loss of *mop-25.2* also caused GCK-1 to become dissipated from apical membranes in both tissues, showing that it has a CASH-1-like effect on localization of the CCM-3/GCK-1 complex to apical membranes. It will be interesting to determine whether MOP-25.2 interacts with the CASH-1 branch of the CCM-3 network to direct CCM-3/GCK-1 to luminal membranes. However, because we did not identify MOP-25.2 as a binding partner of the CCM-3/STRIPAK complex (Pal et al., 2017), it is possible that it might affect the synthesis or stability of CCM-3, which would subsequently alter GCK-1 localization. Although this collectively supports the co-dependency of CCM3 and GCKs in localization to apical membranes (Fidalgo et al., 2010, 2012; Ma et al., 2007; Zhang et al., 2013b), it also reveals a role for MOP-25.2 in the CCM-3/STRIPAK network. Clearly, there is much to learn about the non-canonical roles of MO25/MOP-25.2.

Because it shares a similar function with CCM3 in stress fiber formation in cells, MO25 may be an important determinant of CCM disease. Prevention of stress fiber formation by inhibiting RhoA/ROCK (Richardson et al., 2013; Stockton et al., 2010)

downstream of the hetero-trimeric complex is an attractive therapeutic strategy for managing this disease (McDonald et al., 2012; Shenkar et al., 2017). Our observations suggest that MOP-25.2/MO25 affects the stability of CCM-3/CCM3-containing complexes, and we suspect that the severity of disease in CCM3 patients may be due to its loss from multiple protein complexes. Exploiting the powerful genetics of *C. elegans* has provided insights into how *CCM3* functions *in vivo* and uncovered nodes in this network that might offer therapeutic strategies for managing this disease in humans.

STAR★METHODS

Detailed methods are provided in the online version of this paper and include the following:

- KEY RESOURCES TABLE
- CONTACT FOR REAGENT AND RESOURCE SHARING
- EXPERIMENTAL MODEL AND SUBJECT DETAILS
  - *Caenorhabditis elegans* strains and maintenance
  - Endothelial cell growth conditions
- METHOD DETAILS
  - RNA interference
  - Whole Genome RNAi Screen
  - *C. elegans* microscopy
  - Bioinformatics
  - Cell spreading and immunofluorescence
- QUANTIFICATION AND STATISTICAL ANALYSIS

SUPPLEMENTAL INFORMATION

Supplemental Information includes five figures and four tables and can be found with this article online at https://doi.org/10.1016/j.celrep.2018.08.039.

ACKNOWLEDGMENTS

W.B.D. was supported by the Natural Sciences and Engineering Research Council (RGPIN-2016-06638) and the Canadian Institutes of Health Research (PJT 153000). B.L. was supported by a Restracomp fellowship from the Hospital for Sick Children Research Institute. Strains were provided by the *Caenorhabditis* Genetics Center (funded by the NIH Office of Research Infrastructure Programs [P40 OD010440]). We are grateful to Dr. Salim Seyfried, Dr. Ian Scott, Dr. Anne-Claude Gingras, and Dr. Gary Bader for insightful comments.

AUTHOR CONTRIBUTIONS

B.L. performed experiments, analyzed and assembled data, contributed to project design, and wrote the manuscript. S.P. and E.M.C. performed germline experiments. E.F. performed endothelial cell experiments, and analysis with support from C.A.-R. B.Y. contributed to the generation of transgenic strains and optimized screening with B.L. B.L., S.P., B.Y., D.W., S.C., and L.Z. performed the whole-genome screen. W.B.D. conceived and directed the project and contributed to manuscript writing.

DECLARATION OF INTERESTS

The authors declare no competing interests.

Received: February 16, 2018
Revised: June 27, 2018
Accepted: August 15, 2018
Published: September 11, 2018

REFERENCES

Abdus-Saboor, I., Mancuso, V.P., Murray, J.I., Palozola, K., Norris, C., Hall, D.H., Howell, K., Huang, K., and Sundaram, M.V. (2011). Notch and Ras promote sequential steps of excretory tube development in *C. elegans*. Development *138*, 3545–3555.

Abu Taha, A., and Schnittler, H.-J. (2014). Dynamics between actin and the VE-cadherin/catenin complex: novel aspects of the ARP2/3 complex in regulation of endothelial junctions. Cell Adhes. Migr. *8*, 125–135.

Armenti, S.T., Chan, E., and Nance, J. (2014). Polarized exocyst-mediated vesicle fusion directs intracellular lumenogenesis within the C. elegans excretory cell. Dev. Biol. *394*, 110–121.

Borikova, A.L., Dibble, C.F., Sciaky, N., Welch, C.M., Abell, A.N., Bencharit, S., and Johnson, G.L. (2010). Rho kinase inhibition rescues the endothelial cell cerebral cavernous malformation phenotype. J. Biol. Chem. *285*, 11760–11764.

Boudeau, J., Baas, A.F., Deak, M., Morrice, N.A., Kieloch, A., Schutkowski, M., Prescott, A.R., Clevers, H.C., and Alessi, D.R. (2003). MO25α/β interact with STRADalpha/β enhancing their ability to bind, activate and localize LKB1 in the cytoplasm. EMBO J. *22*, 5102–5114.

Boudeau, J., Scott, J.W., Resta, N., Deak, M., Kieloch, A., Komander, D., Hardie, D.G., Prescott, A.R., van Aalten, D.M.F., and Alessi, D.R. (2004). Analysis of the LKB1-STRAD-MO25 complex. J. Cell Sci. *117*, 6365–6375.

Brenner, S. (1974). The genetics of Caenorhabditis elegans. Genetics *77*, 71–94.

Buechner, M., Hall, D.H., Bhatt, H., and Hedgecock, E.M. (1999). Cystic canal mutants in Caenorhabditis elegans are defective in the apical membrane domain of the renal (excretory) cell. Dev. Biol. *214*, 227–241.

Ceccarelli, D.F., Laister, R.C., Mulligan, V.K., Kean, M.J., Goudreault, M., Scott, I.C., Derry, W.B., Chakrabartty, A., Gingras, A.C., and Sicheri, F. (2011). CCM3/PDCD10 heterodimerizes with germinal center kinase III (GCKIII) proteins using a mechanism analogous to CCM3 homodimerization. J. Biol. Chem. *286*, 25056–25064.

Chien, S.C., Brinkmann, E.M., Teuliere, J., and Garriga, G. (2013). Caenorhabditis elegans PIG-1/MELK acts in a conserved PAR-4/LKB1 polarity pathway to promote asymmetric neuroblast divisions. Genetics *193*, 897–909.

Denning, D.P., Hatch, V., and Horvitz, H.R. (2012). Programmed elimination of cells by caspase-independent cell extrusion in C. elegans. Nature *488*, 226–230.

Draheim, K.M., Li, X., Zhang, R., Fisher, O.S., Villari, G., Boggon, T.J., and Calderwood, D.A. (2015). CCM2-CCM3 interaction stabilizes their protein expression and permits endothelial network formation. J. Cell Biol. *208*, 987–1001.

Fay, D.S. (2008). Classical genetics goes high-tech. Nat. Methods *5*, 863–864.

Fidalgo, M., Fraile, M., Pires, A., Force, T., Pombo, C., and Zalvide, J. (2010). CCM3/PDCD10 stabilizes GCKIII proteins to promote Golgi assembly and cell orientation. J. Cell Sci. *123*, 1274–1284.

Fidalgo, M., Guerrero, A., Fraile, M., Iglesias, C., Pombo, C.M., and Zalvide, J. (2012). Adaptor protein cerebral cavernous malformation 3 (CCM3) mediates phosphorylation of the cytoskeletal proteins ezrin/radixin/moesin by mammalian Ste20-4 to protect cells from oxidative stress. J. Biol. Chem. *287*, 11556–11565.

Filippi, B.M., de los Heros, P., Mehellou, Y., Navratilova, I., Gourlay, R., Deak, M., Plater, L., Toth, R., Zeqiraj, E., and Alessi, D.R. (2011). MO25 is a master regulator of SPAK/OSR1 and MST3/MST4/YSK1 protein kinases. EMBO J. *30*, 1730–1741.

Fischer, A., Zalvide, J., Faurobert, E., Albiges-Rizo, C., and Tournier-Lasserve, E. (2013). Cerebral cavernous malformations: from CCM genes to endothelial cell homeostasis. Trends Mol. Med. *19*, 302–308.

Glading, A.J., and Ginsberg, M.H. (2010). Rap1 and its effector KRIT1/CCM1 regulate beta-catenin signaling. Dis. Model. Mech. *3*, 73–83.

Gumienny, T.L., Lambie, E., Hartwieg, E., Horvitz, H.R., and Hengartner, M.O. (1999). Genetic control of programmed cell death in the Caenorhabditis elegans hermaphrodite germline. Development *126*, 1011–1022.

Hawley, S.A., Boudeau, J., Reid, J.L., Mustard, K.J., Udd, L., Mäkelä, T.P., Alessi, D.R., and Hardie, D.G. (2003). Complexes between the LKB1 tumor suppressor, STRAD alpha/beta and MO25 alpha/beta are upstream kinases in the AMP-activated protein kinase cascade. J. Biol. *2*, 28.

Hwang, J., and Pallas, D.C. (2014). STRIPAK complexes: structure, biological function, and involvement in human diseases. Int. J. Biochem. Cell Biol. *47*, 118–148.

Ito, S., Greiss, S., Gartner, A., and Derry, W.B. (2010). Cell-nonautonomous regulation of C. elegans germ cell death by kri-1. Curr. Biol. *20*, 333–338.

Kamath, R.S., Martinez-Campos, M., Zipperlen, P., Fraser, A.G., and Ahringer, J. (2001). Effectiveness of specific RNA-mediated interference through ingested double-stranded RNA in Caenorhabditis elegans. Genome Biol. *2*, RESEARCH0002.

Kean, M.J., Ceccarelli, D.F., Goudreault, M., Sanches, M., Tate, S., Larsen, B., Gibson, L.C.D., Derry, W.B., Scott, I.C., Pelletier, L., et al. (2011). Structure-function analysis of core STRIPAK Proteins: a signaling complex implicated in Golgi polarization. J. Biol. Chem. *286*, 25065–25075.

Lant, B., Yu, B., Goudreault, M., Holmyard, D., Knight, J.D.R., Xu, P., Zhao, L., Chin, K., Wallace, E., Zhen, M., et al. (2015). CCM-3/STRIPAK promotes seamless tube extension through endocytic recycling. Nat. Commun. *6*, 6449.

Ma, X., Zhao, H., Shan, J., Long, F., Chen, Y., Chen, Y., Zhang, Y., Han, X., and Ma, D. (2007). PDCD10 interacts with Ste20-related kinase MST4 to promote cell growth and transformation via modulation of the ERK pathway. Mol. Biol. Cell *18*, 1965–1978.

Mattingly, B.C., and Buechner, M. (2011). The FGD homologue EXC-5 regulates apical trafficking in C. elegans tubules. Dev. Biol. *359*, 59–72.

McDonald, D.A., Shi, C., Shenkar, R., Stockton, R.A., Liu, F., Ginsberg, M.H., Marchuk, D.A., and Awad, I.A. (2012). Fasudil decreases lesion burden in a murine model of cerebral cavernous malformation disease. Stroke *43*, 571–574.

McGary, K.L., Park, T.J., Woods, J.O., Cha, H.J., Wallingford, J.B., and Marcotte, E.M. (2010). Systematic discovery of nonobvious human disease models through orthologous phenotypes. Proc. Natl. Acad. Sci. U S A *107*, 6544–6549.

Meier, B., Cooke, S.L., Weiss, J., Bailly, A.P., Alexandrov, L.B., Marshall, J., Raine, K., Maddison, M., Anderson, E., Stratton, M.R., et al. (2014). C. elegans whole-genome sequencing reveals mutational signatures related to carcinogens and DNA repair deficiency. Genome Res. *24*, 1624–1636.

Mostafavi, S., Ray, D., Warde-Farley, D., Grouios, C., and Morris, Q. (2008). GeneMANIA: a real-time multiple association network integration algorithm for predicting gene function. Genome Biol. *9* (*Suppl 1*), S4.

Narbonne, P., and Roy, R. (2009). Caenorhabditis elegans dauers need LKB1/AMPK to ration lipid reserves and ensure long-term survival. Nature *457*, 210–214.

Narbonne, P., Hyenne, V., Li, S., Labbé, J.-C., and Roy, R. (2010). Differential requirements for STRAD in LKB1-dependent functions in C. elegans. Development *137*, 661–670.

Nelson, F.K., and Riddle, D.L. (1984). Functional study of the Caenorhabditis elegans secretory-excretory system using laser microsurgery. J. Exp. Zool. *231*, 45–56.

Oliver, A.W., He, X., Borthwick, K., Donne, A.J., Hampson, L., and Hampson, I.N. (2011). The HPV16 E6 binding protein Tip-1 interacts with ARHGEF16, which activates Cdc42. Br. J. Cancer *104*, 324–331.

Pal, S., Lant, B., Yu, B., Tian, R., Tong, J., Krieger, J.R., Moran, M.F., Gingras, A.C., and Derry, W.B. (2017). CCM-3 promotes C. elegans germline development by regulating vesicle trafficking cytokinesis and polarity. Curr. Biol. *27*, 868–876.

Richardson, B.T., Dibble, C.F., Borikova, A.L., and Johnson, G.L. (2013). Cerebral cavernous malformation is a vascular disease associated with activated RhoA signaling. Biol. Chem. *394*, 35–42.

Shenkar, R., Shi, C., Rebeiz, T., Stockton, R.A., McDonald, D.A., Mikati, A.G., Zhang, L., Austin, C., Akers, A.L., Gallione, C.J., et al. (2015). Exceptional aggressiveness of cerebral cavernous malformation disease associated with PDCD10 mutations. Genet. Med. *17*, 188–196.

Shenkar, R., Shi, C., Austin, C., Moore, T., Lightle, R., Cao, Y., Zhang, L., Wu, M., Zeineddine, H.A., Girard, R., et al. (2017). RhoA kinase inhibition with fasudil versus simvastatin in murine models of cerebral cavernous malformations. Stroke *48*, 187–194.

Silverman, G.A., Luke, C.J., Bhatia, S.R., Long, O.S., Vetica, A.C., Perlmutter, D.H., and Pak, S.C. (2009). Modeling molecular and cellular aspects of human disease using the nematode Caenorhabditis elegans. Pediatr. Res. *65*, 10–18.

Sin, O., Michels, H., and Nollen, E.A.A. (2014). Genetic screens in Caenorhabditis elegans models for neurodegenerative diseases. Biochim. Biophys. Acta *1842*, 1951–1959.

Stockton, R.A., Shenkar, R., Awad, I.A., and Ginsberg, M.H. (2010). Cerebral cavernous malformations proteins inhibit Rho kinase to stabilize vascular integrity. J. Exp. Med. *207*, 881–896.

Storkebaum, E., Quaegebeur, A., Vikkula, M., and Carmeliet, P. (2011). Cerebrovascular disorders: molecular insights and therapeutic opportunities. Nat. Neurosci. *14*, 1390–1397.

Sundaram, M.V., and Buechner, M. (2016). The Caenorhabditis elegans excretory system: a model for tubulogenesis, cell fate specification, and plasticity. Genetics *203*, 35–63.

Tojkander, S., Gateva, G., and Lappalainen, P. (2012). Actin stress fibers—assembly, dynamics and biological roles. J. Cell Sci. *125*, 1855–1864.

von Mering, C., Jensen, L.J., Snel, B., Hooper, S.D., Krupp, M., Foglierini, M., Jouffre, N., Huynen, M.A., and Bork, P. (2005). STRING: known and predicted protein-protein associations, integrated and transferred across organisms. Nucleic Acids Res. *33*, D433–D437.

Walck-Shannon, E., Lucas, B., Chin-Sang, I., Reiner, D., Kumfer, K., Cochran, H., Bothfeld, W., and Hardin, J. (2016). CDC-42 orients cell migration during epithelial intercalation in the Caenorhabditis elegans epidermis. PLoS Genet. *12*, e1006415.

Whitehead, K.J., Chan, A.C., Navankasattusas, S., Koh, W., London, N.R., Ling, J., Mayo, A.H., Drakos, S.G., Jones, C.A., Zhu, W., et al. (2009). The cerebral cavernous malformation signaling pathway promotes vascular integrity via Rho GTPases. Nat. Med. *15*, 177–184.

Yin, H., Shi, Z., Jiao, S., Chen, C., Wang, W., Greene, M.I., and Zhou, Z. (2012). Germinal center kinases in immune regulation. Cell. Mol. Immunol. *9*, 439–445.

Yoruk, B., Gillers, B.S., Chi, N.C., and Scott, I.C. (2012). Ccm3 functions in a manner distinct from Ccm1 and Ccm2 in a zebrafish model of CCM vascular disease. Dev. Biol. *362*, 121–131.

You, C., Sandalcioglu, I.E., Dammann, P., Felbor, U., Sure, U., and Zhu, Y. (2013). Loss of CCM3 impairs DLL4-Notch signalling: implication in endothelial angiogenesis and in inherited cerebral cavernous malformations. J. Cell. Mol. Med. *17*, 407–418.

You, C., Zhao, K., Dammann, P., Keyvani, K., Kreitschmann-Andermahr, I., Sure, U., and Zhu, Y. (2017). EphB4 forward signalling mediates angiogenesis caused by CCM3/PDCD10-ablation. J. Cell. Mol. Med. *21*, 1848–1858.

Zhang, M., Dong, L., Shi, Z., Jiao, S., Zhang, Z., Zhang, W., Liu, G., Chen, C., Feng, M., Hao, Q., et al. (2013a). Structural mechanism of CCM3 heterodimerization with GCKIII kinases. Structure *21*, 680–688.

Zhang, Y., Tang, W., Zhang, H., Niu, X., Xu, Y., Zhang, J., Gao, K., Pan, W., Boggon, T.J., Toomre, D., et al. (2013b). A network of interactions enables CCM3 and STK24 to coordinate UNC13D-driven vesicle exocytosis in neutrophils. Dev. Cell *27*, 215–226.

Zheng, X., Xu, C., Di Lorenzo, A., Kleaveland, B., Zou, Z., Seiler, C., Chen, M., Cheng, L., Xiao, J., He, J., et al. (2010). CCM3 signaling through sterile 20-like kinases plays an essential role during zebrafish cardiovascular development and cerebral cavernous malformations. J. Clin. Invest. *120*, 2795–2804.

Zhou, Z., Rawnsley, D.R., Goddard, L.M., Pan, W., Cao, X.J., Jakus, Z., Zheng, H., Yang, J., Arthur, J.S.C., Whitehead, K.J., et al. (2015). The cerebral cavernous malformation pathway controls cardiac development via regulation of endocardial MEKK3 signaling and KLF expression. Dev. Cell *32*, 168–180.

Zhou, H.J., Qin, L., Zhang, H., Tang, W., Ji, W., He, Y., Liang, X., Wang, Z., Yuan, Q., Vortmeyer, A., et al. (2016a). Erratum: Endothelial exocytosis of angiopoietin-2 resulting from CCM3 deficiency contributes to cerebral cavernous malformation. Nat. Med. *22*, 1502.

Zhou, Z., Tang, A.T., Wong, W.-Y., Bamezai, S., Goddard, L.M., Shenkar, R., Zhou, S., Yang, J., Wright, A.C., Foley, M., et al. (2016b). Cerebral cavernous malformations arise from endothelial gain of MEKK3-KLF2/4 signalling. Nature *532*, 122–126.

STAR★METHODS

KEY RESOURCES TABLE

REAGENT or RESOURCE	SOURCE	IDENTIFIER
Antibodies		
Anti-VE-Cadherin Antibody (CD144), clone BV9	Millipore Sigma/Merck Millipore	Cat # sc-52751 (RRID: AB_628919)
TRITC-conjugated phalloidin	Sigma Aldrich	FAK100 part 90228
Goat anti-Mouse IgG (H+L) Highly Cross-Adsorbed Secondary Antibody, Alexa Fluor Plus 488	Invitrogen	Cat # A32723 (RRIID: AB_2633275)
Bacterial and Virus Strains		
Caenorhabditis elegans RNAi feeding library	Source Bioscience	https://www.sourcebioscience.com/products/life-science-research/clones/rnai-resources/c-elegans-rnai-collection-ahringer/
OP50 (*E. coli*)	Caenorhabditis Genetics Center	WormBase ID: OP50
Chemicals, Peptides, and Recombinant Proteins		
Ampicillin	Sigma-Aldrich	A1593; CAS Number 69-53-4
Tetracycline hydrochloride	Sigma-Aldrich	T7660; CAS Number 64-75-5
Isopropyl-β-D-thiogalactopyranoside (IPTG)	Sigma-Aldrich	I1284; CAS Number 367-93-1
Tetramisole	Sigma-Aldrich	T1512; CAS Number 5086-74-8
Penicillin/Streptomyocin	Sigma-Aldrich	P4333
Fibronectin Human Plasma	Sigma-Aldrich	F0895
Rat Tail Collagen I	Corning	Product # 354236
Vasculife VEGF Medium	Lifeline Cell Technology	LL-0005
EBM-2 Basal Medium	Lonza	CC-3156
Lipofectamine RNAi max	Life Technologies	ref. 13778-150
Trypsin inhibitor	Sigma-Aldrich	T6522
Mowiol	Sigma-Aldrich	324590
Experimental Models: Cell Lines		
HUVEC-Umbil Vein, Pooled Cells	Lonza	CC-2519, C2519A
Experimental Models: Organisms/Strains		
C. elegans: Strain N2	Caenorhabditis Genetics Center	WormBase ID: N2
C. elegans: Strain BK204: *qpIs96*[P_{exc-9}::mCherry::*cdc-42*]	The Buechner Laboratory	WormBase ID: BK204
C. elegans: Strain BK205: *qpIs97*[P_{exc-9}::mCherry::*rab-11*]V	The Buechner Laboratory	WormBase ID: BK205
C. elegans: Strain BK220: *qpIs103*[P_{exc-9}::mCherry::GRIP]	The Buechner Laboratory	WormBase ID: BK220
C. elegans: Strain BK262: *qpIs104*[P_{exc-9}::mCherry::GBD_{wsp-1}]	The Buechner Laboratory	WormBase ID: BK262
C. elegans: Strain OD95: *unc-119(ed3)* III; ltIs37 [pAA64; *pie-1*::mCherry::HIS-58 + *unc-119(+)*] IV; ltIs38 [pAA1; *pie-1*::GFP::PH(PLC1delta1) + *unc-119(+)*]	Caenorhabditis Genetics Center	WormBase ID: OD95
C. elegans: Strain WD187: *kri-1(ok1251)*I; *bgIs312*{P_{vha-8}::GFP}	The Derry Lab	N/A
C. elegans: Strain WD188: *ccm-3(tm2806)/mIn1[mIs14 dpy-10(e128) let(gk838)]*II; *bgIs312*{P_{vha-8}*::GFP*}	The Derry Lab	N/A
C. elegans: Strain WD355: *onIs3* {P_{ccm-3}::GFP::CCM-3; *unc-119(+)*}II; *unc-119(ed3)* III	The Derry Lab	N/A
C. elegans: Strain WD419: N2*; onEx62[*P_{exc-9}*::ccm-3::GFP*; P_{myo-2}::mCherry*;* P_{myo-3}::mCherry; P_{rab-3}::mCherry]*	The Derry Lab	N/A
C. elegans: Strain WD423: N2*; onEx69[*P_{exc-9}*::ccm-3::*GFP; P_{exc-9}*::gck-1::*mCherry; *rol-6(su1006)]*	The Derry Lab	N/A

(*Continued on next page*)

Continued

REAGENT or RESOURCE	SOURCE	IDENTIFIER
C. elegans: StrainWD472: *gck-1(onIs11 [gck-1*::GFP::*3xFlag+loxP SEC loxP])* III	The Derry Lab	N/A
Oligonucleotides		
siRNA (siCT)	Dharmacon	ref D-001810-01
siRNA (siCCM3)	Dharmacon	ref L-004436-01
siRNA (siMO25)	Dharmacon	ref L-015407-01
Software and Algorithms		
BioMart	Ensembl	http://useast.ensembl.org/biomart/martview/2e75a78fc2af8b2fa42aeeb328b837e9
GeneMania	Jason Montojo/ GeneMania Team (University of Toronto)	https://genemania.org/ and http://apps.cytoscape.org/apps/genemania
ImageJ	Wayne Rasband/ NIH	http://imagej.nih.gov/ij
OpenLAB	Agilent	https://www.agilent.com/en-us/products/software-informatics/openlab-software-suite
STRING	Swiss Institute of Bioinformatics, CPR-NNF Center for Protein Research, and European Molecular Biology Laboratory	https://string-db.org/

CONTACT FOR REAGENT AND RESOURCE SHARING

Further information and requests for resources and reagents should be directed to and will be fulfilled by the Lead Contact, Dr. Brent Derry (brent.derry@sickkids.ca).

EXPERIMENTAL MODEL AND SUBJECT DETAILS

Caenorhabditis elegans strains and maintenance

Worms were cultivated on lawns of *E. coli* (strain OP50) grown on NGM (nematode growth medium) plates at 20°C (unless otherwise stated) (Brenner, 1974). Wild-type (WT) refers to the *C. elegans* variety Bristol, strain N2. Compound mutant and transgenic strains were constructed according to standard *C. elegans* protocols (Fay, 2008). See KRT for strain list. Excretory canal marker strains designated 'BK' were a kind gift from Dr. Matthew Buechner.

Endothelial cell growth conditions

Pooled HUVECs were grown on collagen I coated plates in complete EBM media, supplemented with 100U/ml penicillin and 100 μg/ml streptomycin, at 37°C in a 5% CO2-humidified chamber according to the manufacturer's instructions. HUVEC (1.5×10^6 cells) were transfected twice at 24 h intervals with 20 nM siRNA and 45 μL lipofectamine RNAi max according to the manufacturer's instructions.

METHOD DETAILS

RNA interference

RNAi was performed by feeding bacteria expressing double-stranded RNA (RNAi) to worms at the L1 stage, according to Kamath et al. (Kamath et al., 2001). Bacterial cultures expressing double-stranded RNA targeting the gene of interest were drawn from the Source BioScience RNAi library, and grown on nematode growth media (NGM) plates supplemented with antibiotics (50 μg/ml ampicillin and 12.5 μg/ml tetracycline) and 0.1 mM isopropyl-β-D-thiogalactopyranoside to induce dsRNA production. Bacteria expressing an empty RNAi vector (L4440; within competent HT115 cells) were used as controls. For excretory canals analysis, to decrease variance between worms, RNAi was concentrated 5X, and worms were grown on RNAi bacteria for two generations. In the cases where worms did not survive two full generations of RNAi, L4s were placed on the bacteria, and subsequent F1 progeny were analyzed.

Whole Genome RNAi Screen

We previously observed that ablation of *ccm-3* and *kri-1* causes synthetic lethality (Lant et al., 2015). Hence, we reasoned that other genes that cause synthetic conditions ('sickness') when knocked down in *kri-1(ok1251)* mutants might reveal additional components

of the *ccm-3* pathway. *kri-1(ok1251)* mutants were fed bacteria expressing dsRNA to genes from the Source Bioscience RNAi library in liquid culture format (96 well plates). A 96 pin-replicator was plunged into the wells of a thawed RNAi library plate (4 pins/plates per 384 well library plate), then immersed in 150μl of LB+AMP+TET, aliquoted into each well of a conical tip 96 well plate. The plates were covered in parafilm and a wet paper towel, placed in a sealed plastic bag to prevent evaporation, then incubated on a shaker overnight at 37°C. The following day bacterial cultures were induced with 6μl IPTG (0.1M) per well, and incubated for one more hour. Bacteria was pelleted by centrifugation (3,500rpm) for 5 min, the supernatant removed, and pellets re-suspended in150μl liquid NGM per well. 50μl of this induced bacterial RNAi culture was transferred to a flat-bottom 96 well plate and 10 L1 stage *kri-1(ok1251)* mutant worms were added. The plates were sealed (as above) and placed on an orbital shaker at room temperature and grown 4-5 days. Sickness (embryonic lethality, larval lethality, sterility, and slow growth) of F1 progeny from *kri-1* mutants was assessed and cataloged. Concurrently, N2 (WT) controls were grown in the same RNAi conditions (in separate wells). Negative genetic interactions based on synthetic lethal and sick phenotypes were categorized as those observed in *kri-1* but not N2 controls.

C. elegans microscopy

Nematodes were slide mounted in a 5μl aliquot of tetramisole anesthetic (20-100mM; higher concentration for roller strains), on a flat pad of 4% agar. Nematodes were imaged at 63X or 100X magnification using a Leica DMRA2 compound microscope equipped differential interference contrast (DIC) optics and epifluorescence. Images were captured with a Hamamatsu C472-95 digital camera using Openlab software (PerkinElmer Inc.).

Bioinformatics

A master list of 35 genes (from mammalian CCM literature was converted into gene and protein IDs via BioMart (Ensembl), and then used to generate 'CCM-omes' via GeneMANIA and STRING, respectively. For the gene lists a total of 500 were obtained by selecting for biological relevance using GO term sorting for *GO Biological Process*, *GO Molecular Function*, and *GO Cellular Component* in GeneMANIA. The amalgamated GeneMANIA list (i.e., removing multiple entries for the same genes) amounted to 769 genes. For the protein interaction list STRING was used to generate a list of 500 proteins, using its automatic weighting system. These lists were converted to worm orthologs via BioMart, resulting in 535 independent genes from the GeneMania list and 231 genes from the STRING list. Further amalgamation of these two lists produced a final worm ''CCM-ome'' of 653 genes. The overlapping genes between the 'Sick' list from the RNAi screen (562 genes) and the CCM-ome list (653 genes) were termed ''Tier 1'' hits, which amounted to 29 genes ('Experimental Set') that were examined for canal effects against 29 randomly selected ('Control Set') genes. The ID of Control set genes were generated by assigning a number to each gene in the Source Bioscience RNAi library, and then generating a random list of 29 numbers using the RAND function in Microsoft Excel.

Cell spreading and immunofluorescence

Transfected cells were trypsinized, treated with 1 mg/ml trypsin inhibitor, and incubated in serum-free EBM-2/1% BSA for 30 min at 37°C. Sparse HUVECs (10^4) were spread for 4h on 24-well plates slides coated with 2 μg/ml of Fibronectin (FN), in vasculife VEGF media containing 5% FN-depleted serum and then fixed with 4% PFA. Confluent HUVECs (2×10^5 cells) were seeded in 24-well plates on slides coated with 20 μg/ml FN and incubated for 72h in complete vasculife media. Cells were fixed with 4% PFA, permeabilized with 0.2% Triton X-100, and incubated with VE-cadherin BV9 antibody at 1/200 dilution. After rinsing, coverslips were incubated with an Alexa Fluor 488–conjugated secondary antibody and phalloidin-TRITC. The cells were mounted in Mowiol/DAPI solution and imaged on epifluorescent Axiomager microscope (Zeiss) with AxioCamMRc camera.

QUANTIFICATION AND STATISTICAL ANALYSIS

Significance of the Tier 1 set (29 genes) of hits generated from overlapping genes in the informatics set (653 genes) and the genome screen set (562 genes) was validated through a hypergeometric analysis and was found to be significant ($p = 0.012$). Additionally, randomizing sets of numbers ($n = 10$), the average overlapping values for comparisons of 653 and 562 numbers resulted in 18.2 ± 4.6 (mean ± standard deviation), wherein our value of 29 is outside of two standard deviations.

Excretory canal lengths were measured from excretory cell to the canal tip. These values were normalized by a 'total' length measurement of the worm (excretory cell to anus), with the 'relative' canal length expressed as a percentage according to Lant et al., 2015. Individual canal measurements were plotted in GraphPad Prism, with mean values marked by a red bar.

Germline apoptotic corpse counts were performed 24 hr post IR, following a 60 gy dosage at the young adult stage. Germlines were observed and counted directly at 630X magnification using a Leica DMRA2 compound microscope. Individual germline arm corpse counts were plotted in GraphPad Prism, with mean values marked by a red bar. Values were accumulated from three or more experimental datasets. *P value*s, relative to 'control RNAi' were determined using a two-tailed Student's t test, assuming equal variance. Significance levels (*P value*) and sample size (*N*) are marked in each corresponding figure legend.

Comparison of Control and Experimental sets of data, cumulatively, using a two tailed Student's t test, assuming equal variance, showed the two sets to be significantly different ($p = 6.92762E-36$). Comparison of Control and Experimental sets, as collections of genes with a rating of *no truncation*, *truncation*, or *strong truncation* was conducted using the CHI square test and showed the two groups to have significantly different distributions in these categories ($p = 0.0031$).

Puncta counts and fluorescent signal measurements were obtained using ImageJ software. Puncta counts were measured (Lant et al., 2015) using an RGB profile plot on a stretch of canal (~100μm in length) at or near the posterior distal tip. Each representative image shows a single plane, of one canal, with the maximal amount of puncta present. Relative intensity of GFP/RFP signals were assessed by measuring the requisite RGB channel signal, and normalizing with RGB signal from surrounding tissue (canals), or within the pachytene cells (germline rachis) in which a neutral 'non-signal' holds a value of 1. In each case, values have been compared from the given RNAi type to a control (empty vector) RNAi.

For quantification of the number of cells displaying transversal actin fibers (stress fiber) above their nucleus, more than 100 cells per phenotype in 3 independent experiments were counted, and the relative frequency of stress fiber presence was normalized for control siRNA numbers.